

Measurement of Nuclear Transparency Ratios for Protons and Neutrons

M. Duer,¹ O. Hen,^{2,*} E. Piassetzky,¹ L.B. Weinstein,³ A. Schmidt,² I. Korover,¹ E. O. Cohen,¹ H. Hakobyan,⁴ S. Adhikari,¹⁵ G. Angelini,¹⁸ H. Avakian,⁴⁰ L. Barion,²⁰ M. Battaglieri,²² A. Beck,^{2,†} I. Bedlinskiy,²⁶ A.S. Biselli,^{13,7} S. Boiarinov,⁴⁰ W.J. Briscoe,¹⁸ W. Brooks,⁴ V.D. Burkert,⁴⁰ F. Cao,¹¹ D.S. Carman,⁴⁰ A. Celentano,²² P. Chatagnon,²⁵ T. Chetry,³³ G. Ciullo,^{20,14} P.L. Cole,^{29,19,8} M. Contalbrigo,²⁰ O. Cortes,¹⁸ V. Crede,¹⁶ R. Cruz Torres,² A. D'Angelo,^{23,36} N. Dashyan,⁴⁵ R. De Vita,²² E. De Sanctis,²¹ A. Deur,⁴⁰ S. Diehl,¹¹ C. Djalali,^{33,38} R. Dupre,²⁵ Burcu Duran,³⁹ H. Egiyan,⁴⁰ M. Ehrhart,²⁵ A. El Alaoui,⁴ L. El Fassi,³⁰ P. Eugenio,¹⁶ A. Filippi,²⁴ T.A. Forest,¹⁹ G.P. Gilfoyle,³⁵ F.X. Girod,⁴⁰ E. Golovatch,³⁷ R.W. Gothe,³⁸ K.A. Griffioen,⁴⁴ M. Guidal,²⁵ L. Guo,^{15,40} K. Hafidi,⁵ C. Hanretty,⁴⁰ N. Harrison,⁴⁰ M. Hattawy,³ F. Hauenstein,³ T.B. Hayward,⁴⁴ D. Heddle,^{10,40} M. Holtrop,³¹ Y. Ilieva,^{38,18} D.G. Ireland,⁴¹ B.S. Ishkhanov,³⁷ E.L. Isupov,³⁷ H.S. Jo,²⁸ S. Johnston,⁵ K. Joo,¹¹ S. Joosten,³⁹ D. Keller,⁴³ G. Khachatryan,⁴⁵ M. Khachatryan,³ A. Khanal,¹⁵ M. Khandaker,^{32,‡} A. Kim,¹¹ W. Kim,²⁸ A. Klein,³ F.J. Klein,⁸ V. Kubarovsky,^{40,34} S.E. Kuhn,³ S.V. Kuleshov,^{4,26} L. Lanza,²³ G. Laskaris,² P. Lenisa,²⁰ K. Livingston,⁴¹ I. J. D. MacGregor,⁴¹ D. Marchand,²⁵ B. McKinnon,⁴¹ S. Mey-Tal Beck,^{2,†} T. Mineeva,⁴ M. Mirazita,²¹ V. Mokeev,^{40,37} R.A. Montgomery,⁴¹ A. Movsisyan,²⁰ C. Munoz Camacho,²⁵ B. Mustapha,⁵ P. Nadel-Turonski,⁴⁰ S. Niccolai,²⁵ G. Niculescu,²⁷ M. Osipenko,²² A.I. Ostrovidov,¹⁶ M. Paolone,³⁹ L.L. Pappalardo,²⁰ R. Paremuzyan,³¹ E. Pasyuk,^{40,6} M. Patsyuk,² D. Payette,³ J. Price,⁴⁶ D. Pocanic,⁴³ O. Pogorelko,²⁶ Y. Prok,^{3,43} D. Protopopescu,⁴¹ B.A. Raue,^{15,40} M. Ripani,²² D. Riser,¹¹ A. Rizzo,^{23,36} G. Rosner,⁴¹ P. Rossi,^{40,21} F. Sabatié,⁹ C. Salgado,³² B.A. Schmookler,² R.A. Schumacher,⁷ Y.G. Sharabian,⁴⁰ Iu. Skorodumina,^{38,37} D. Sokhan,⁴¹ O. Soto,⁴ N. Sparveris,³⁹ S. Stepanyan,⁴⁰ S. Strauch,^{38,18} M. Taiuti,^{17,§} J.A. Tan,²⁸ M. Ungaro,^{40,34} H. Voskanyan,⁴⁵ E. Voutier,²⁵ R. Wang,²⁵ X. Wei,⁴⁰ N. Zachariou,⁴² J. Zhang,⁴³ Z.W. Zhao,¹² and X. Zheng⁴³

(The CLAS Collaboration)

¹*School of Physics and Astronomy, Tel Aviv University, Tel Aviv 69978, Israel*

²*Massachusetts Institute of Technology, Cambridge, Massachusetts 02139, USA*

³*Old Dominion University, Norfolk, Virginia 23529*

⁴*Universidad Técnica Federico Santa María, Casilla 110-V Valparaíso, Chile*

⁵*Argonne National Laboratory, Argonne, Illinois 60439*

⁶*Arizona State University, Tempe, Arizona 85287-1504*

⁷*Carnegie Mellon University, Pittsburgh, Pennsylvania 15213*

⁸*Catholic University of America, Washington, D.C. 20064*

⁹*IRFU, CEA, Université Paris-Saclay, F-91191 Gif-sur-Yvette, France*

¹⁰*Christopher Newport University, Newport News, Virginia 23606*

¹¹*University of Connecticut, Storrs, Connecticut 06269*

¹²*Duke University, Durham, North Carolina 27708-0305*

¹³*Fairfield University, Fairfield CT 06824*

¹⁴*Università di Ferrara, 44121 Ferrara, Italy*

¹⁵*Florida International University, Miami, Florida 33199*

¹⁶*Florida State University, Tallahassee, Florida 32306*

¹⁷*Università di Genova, 16146 Genova, Italy*

¹⁸*The George Washington University, Washington, DC 20052*

¹⁹*Idaho State University, Pocatello, Idaho 83209*

²⁰*INFN, Sezione di Ferrara, 44100 Ferrara, Italy*

²¹*INFN, Laboratori Nazionali di Frascati, 00044 Frascati, Italy*

²²*INFN, Sezione di Genova, 16146 Genova, Italy*

²³*INFN, Sezione di Roma Tor Vergata, 00133 Rome, Italy*

²⁴*INFN, Sezione di Torino, 10125 Torino, Italy*

²⁵*Institut de Physique Nucléaire, IN2P3-CNRS, Université Paris-Sud, Université Paris-Saclay, F-91406 Orsay, France*

²⁶*Institute of Theoretical and Experimental Physics, Moscow, 117259, Russia*

²⁷*James Madison University, Harrisonburg, Virginia 22807*

²⁸*Kyungpook National University, Daegu 41566, Republic of Korea*

²⁹*Lamar University, 4400 MLK Blvd, PO Box 10009, Beaumont, Texas 77710*

³⁰*Mississippi State University, Mississippi State, MS 39762-5167*

³¹*University of New Hampshire, Durham, New Hampshire 03824-3568*

³²*Norfolk State University, Norfolk, Virginia 23504*

³³*Ohio University, Athens, Ohio 45701*

³⁴*Rensselaer Polytechnic Institute, Troy, New York 12180-3590*

³⁵*University of Richmond, Richmond, Virginia 23173*

³⁶*Universita' di Roma Tor Vergata, 00133 Rome Italy*

³⁷*Skobeltsyn Institute of Nuclear Physics, Lomonosov Moscow State University, 119234 Moscow, Russia*

³⁸*University of South Carolina, Columbia, South Carolina 29208*

³⁹*Temple University, Philadelphia, PA 19122*

⁴⁰*Thomas Jefferson National Accelerator Facility, Newport News, Virginia 23606*

⁴¹*University of Glasgow, Glasgow G12 8QQ, United Kingdom*

⁴²*University of York, York YO10, United Kingdom*

⁴³*University of Virginia, Charlottesville, Virginia 22901*

⁴⁴*College of William and Mary, Williamsburg, Virginia 23187-8795*

⁴⁵*Yerevan Physics Institute, 375036 Yerevan, Armenia*

⁴⁶*California State University Dominguez Hills, Carson, CA 90747*

This paper presents, for the first time, measurements of neutron transparency ratios for nuclei relative to C measured using the $(e, e'n)$ reaction, spanning measured neutron momenta of 1.4 to 2.4 GeV/c. The transparency ratios were extracted in two kinematical regions, corresponding to knockout of mean-field nucleons and to the breakup of Short-Range Correlated nucleon pairs. The extracted neutron transparency ratios are consistent with each other for the two measured kinematical regions and agree with the proton transparencies extracted from new and previous $(e, e'p)$ measurements, including those from neutron-rich nuclei such as lead. The data also agree with and confirm the Glauber approximation that is commonly used to interpret experimental data. The nuclear-mass-dependence of the extracted transparencies scales as A^α with $\alpha = -0.289 \pm 0.007$, which is consistent with nuclear-surface dominance of the reactions.

PACS numbers:

High-energy, large-momentum-transfer electron scattering reactions are used to study a wide range of nuclear phenomena from the shell-structure of nuclei to partonic color transparency effects for nucleons. The interpretation of these measurements relies on models of the electron interaction cross-section. The nuclear transparency factor, $T(A)$, describes the probability of the outgoing nucleon to emerge from the nucleus, quantifying the multiple scattering of the knockout nucleon with the surrounding nucleons. $T(A)$ is a key ingredient in many calculations of nuclear reactions.

Nuclear transparency, calculated using the Glauber approximation, is widely used in the analyses of reactions measured in high-energy, heavy-ion, and hadronic physics experiments. Therefore, the experimental extraction of transparency factors for single nucleon knockout reactions at different kinematics and for different nuclei serves as an important baseline for obtaining information on the structure and dynamics of individual nucleons bound in nuclei and as a detailed benchmark for the validity of the widely used Glauber calculations. See [1] for a recent review.

We present an experimental extraction of the transparency ratios, $T(A)/T(^{12}\text{C})$, for proton and neutron knockout, from measurements of Quasi-Elastic (QE) $A(e, e'n)$ and $A(e, e'p)$ reactions. Here A represents carbon, aluminum, iron, and lead (or their corresponding atomic numbers). The carbon nucleus was chosen as a reference because it is a well-studied symmetric nucleus. The transparency ratios were extracted in two kinematic regimes, the first corresponding to the knockout of Mean-Field (MF) nucleons and the second corresponding to the knockout of nucleons from Short-Range Correlated (SRC) nucleon pairs [2]. In both regimes, a requirement

of large momentum transfer ($Q^2 \geq 1.5 \text{ GeV}^2$) was enforced, which constrained the detected nucleon momentum to be greater than 1.4 GeV/c.

In MF kinematics, the reconstructed initial momenta of the knockout nucleons are below the nuclear Fermi momentum, where the nuclear spectral functions are relatively well-modeled. In SRC kinematics, the reconstructed initial momenta of the knockout nucleons are greater than the nuclear Fermi momentum because the nucleons are members of SRC pairs [2].

The extracted transparencies for the two kinematics are consistent with each other within their experimental uncertainties. The neutron knockout transparencies, obtained here for the first time, are also consistent with the proton knockout transparencies, even in nuclei such as lead, which has about 1.5 times more neutrons than protons. The A -dependences of the neutron- and proton-knockout transparencies show a power-law scaling of A^α , with $\alpha = -0.289 \pm 0.007$. This exponent is consistent with $-1/3$, the value expected for scattering from the nuclear surface. Moreover, the proton knockout data agree with Glauber calculations, validating their use in analyses of high-energy nuclear reactions. While Glauber calculations of neutron knockout reactions are unavailable at the moment, they should not significantly deviate from the proton knockout calculations in order to be consistent with the data presented here.

The analysis presented here was carried out as part of the Thomas Jefferson National Accelerator Facility (JLab) Hall B Data-Mining project [3] using data from the Experiments E02-104 and E02-110, which took place in 2004 in Hall B at JLab. The experiments used a 5.01 GeV unpolarized electron beam incident on a dedicated target system [4]. Scattered electrons and knockout nu-

cleons were detected using the CEBAF Large Acceptance Spectrometer (CLAS) [5].

CLAS consisted of a toroidal super-conducting magnet and six independent sectors containing sets of drift chambers (DC), time-of-flight scintillation counters (TOF), Cherenkov counters (CC), and electro-magnetic calorimeters (EC) for trajectory reconstruction and particle identification. The polar angular acceptance was $8^\circ < \theta < 140^\circ$. The azimuthal angular acceptance was 50% at small polar angles, increasing to 80% at larger polar angles.

The specially designed target consisted of a liquid deuterium (LD₂) cryotarget, followed by one of five independently-installable solid targets ranging in thickness from 0.16 g/cm² to 0.32 g/cm² (thin and thick Al, C, Fe, and Pb, all in natural isotopic abundances) [4]. The LD₂ target cell and the solid targets were separated by about 4 cm. We selected events with particles scattering from the solid target by reconstructing the intersections of their trajectories with the beam line. The vertex reconstruction resolution for both electrons and protons was sufficient to unambiguously separate particles originating from the cryotarget and the solid target. The analysis presented here used only data from the solid targets.

Scattered electrons were identified and pions rejected by requiring negatively-charged tracks that produced more than 2.5 photo-electrons in the CC with energy deposits in the inner and outer parts of the EC that are correlated and proportional to the particle momentum [5]. Neutrons were identified by observing interactions in the forward EC (covering polar angles from 8° to 45°), with no associated hit in the preceding TOF bar and no charged-particle tracks in the DC. We only considered interactions that were within the fiducial region of the EC, defined to include only hits reconstructed within 10 cm from its edge. The angle- and momentum-dependent neutron detection efficiency and momentum reconstruction resolution were determined simultaneously using the exclusive $d(e, e'p\pi^+\pi^-)n$ and $d(e, e'p\pi^+\pi^-)n$ reactions [6, 7]. Protons in CLAS were identified by requiring that the difference between the measured time of flight and that calculated from the measured momentum and the nominal proton mass be within two standard deviations from the mean of the event distribution over that difference. This cut clearly separates protons from pions and kaons up to a momentum of 2.8 GeV/c.

We applied fiducial cuts on the angles and momenta of all charged particles to avoid regions with steeply varying acceptance close to the magnetic coils of CLAS and the edges of the detectors. The fiducial region for neutron detection was defined by the EC fiducial region as described above. In order to match the knockout nucleon acceptances in the $A(e, e'p)$ and the $A(e, e'n)$ reactions, we considered only protons emerging from the nucleus at angles that are within the fiducial regions for neutrons.

We then applied the proton fiducial cuts on the detected neutrons. Also, we considered only protons with momenta up to 2.4 GeV/c, in order to match the maximal neutron momentum considered in the analysis [6, 7].

We corrected the kinetic energy of the incoming electron and of the scattered electron and proton for Coulomb distortions on an event-by-event basis using the Effective Momentum Approximation (EMA) [8]. Following [9], we assumed an effective electric potential equal to 75% of the potential produced by Z unscreened charges located at the center of the nucleus. This amounts to a 3-, 5-, 10- and 20-MeV correction for C, Al, Fe, and Pb, respectively [10, 11].

In QE electron-scattering processes, within the one-body, one-photon exchange approximation, the momentum and the energy transfer to the virtual photon are absorbed by a single nucleon with an initial momentum \vec{p}_i , leaving the undetected (missing) residual $(A-1)$ system with excitation energy $E_{miss} = \omega - T_N - T_{A-1}$, where ω is the virtual-photon energy transfer, T_N is the kinetic energy of the detected nucleon, and T_{A-1} is the reconstructed kinetic energy of the residual $A-1$ system. The missing momentum is $p_{miss} = |\vec{p}_N - \vec{q}|$, where \vec{p}_N is the measured nucleon momentum and \vec{q} is the momentum of the virtual photon. Using this definition, in the Plane Wave Impulse Approximation (PWIA), the initial momentum of the struck nucleon p_i is equal to p_{miss} .

The identification of $A(e, e'N)$ events (in which N stands for either proton or neutron) in either MF or SRC kinematics, follows previous work [7, 10, 11]. For the MF kinematics, this includes selection of events with $Q^2 > 1.5$ GeV², and low missing energy and momentum: $E_{miss} < 80 - 90$ MeV and $p_{miss} < 250$ MeV/c [12–14] and $-0.05 < y < 0.25$. The latter is a scaling variable that is related to the component of the initial momentum of the knocked-out nucleon in the direction of the momentum transfer vector [15]. For QE events y is expected to be centered around zero. In this analysis it is shifted to small positive values due to the limited angular acceptance of the EC. For the SRC kinematics, this includes selection of events with $x_B > 1.2$, which leads to choosing a nucleon with momentum of relative magnitude in the range $0.62 < |\vec{p}_N|/|\vec{q}| < 0.96$ and direction similar to that of the virtual photon ($\theta_{Nq} < 25^\circ$). Also, in SRC kinematics, we required that the missing momentum was high ($p_{miss} > 300$ MeV/c) [10].

Although these event-selection cuts proved effective for studies of $(e, e'p)$ reactions in the two relevant kinematics, in the case of $(e, e'n)$ the neutron momentum-reconstruction resolution was insufficient to directly distinguish between events with high and low missing momentum and energy. To overcome this issue, we developed an alternative set of cuts that makes use only of quantities insensitive to the poor neutron momentum-reconstruction resolution, such as the momentum of the scattered electron and the direction of the knockout nu-

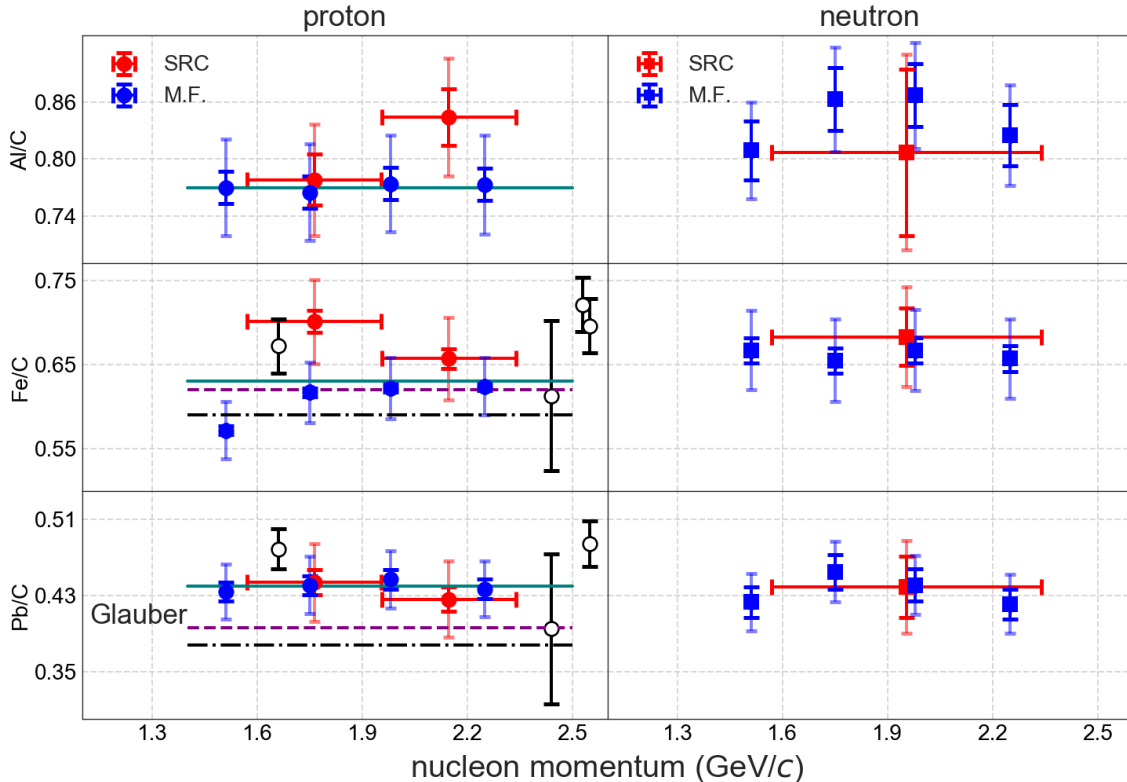


FIG. 1: The estimated transparency ratios for MF and SRC kinematics, both for protons and neutrons, as a function of the nucleon momentum. Inner error bars are statistical and outer error bars include statistical and systematics uncertainties, the latter are common for the different data-points of a given measurement. The black open circles show the world data for the transparency ratios for MF proton knockout from Ref. [13, 14, 16, 17]. Glauber calculations are shown as dotted [18], dashed [19], and solid [20, 21] lines. The nucleon momentum range for the SRC data points is denoted by the horizontal line round each point, while that of the MF data points is the same for all points and is not shown for clarity.

clean. This alternative set of cuts was chosen to select an event sample as similar as possible to the nominal set, with reduced sensitivity to the neutron momentum reconstruction resolution [7].

The development of these alternative selection cuts required analyzing a data-driven Monte-Carlo ($e, e'p$) event sample, in which each measured event was used to generate several events for which the measured momentum of the proton was smeared according to the neutron momentum resolution. For each generated event, all related kinematical variables, such as missing momentum and energy, were calculated twice, using the proton measured and smeared momentum. This allowed us to estimate the efficiency and purity of the alternative selection cuts when applied to ($e, e'n$) events.

The alternative selection cuts are listed in Table I and II for the MF and SRC kinematics, respectively. In both cases, the alternative cuts were chosen such that the selection efficiency is as large as possible while background

contamination by other events is minimal. The efficiency of the alternative cuts is about 90% in either kinematics, with a contamination of about 10%, making the total event sample sizes equivalent to those obtained using the unsmear momentum and the nominal selection cuts (MF and SRC).

Using the selected event samples, we then extract the cross-section ratios for scattering off the solid targets relative to carbon. The cross-section ratios are defined as the normalized-yield ratios, where each yield is normalized to the number of scattering centers (number of protons or number of neutrons) in the target and the total number of electrons incident on the corresponding target during the experiment. Detector acceptance effects cancel in the cross-section ratios because (a) all solid targets were located at the same position on the beam line and (b) the shapes of the event distributions giving the yields in the nominator and the denominator of each transparency ratio, were observed to be similar for the

final-state kinematical variables for the different targets (including missing energy and momentum).

The $A(e, e'N)$ cross-section ratios were corrected for radiative effects [22] in the same way as was done in [10, 23, 24]. The radiative correction to the transparency ratio was found to be $\sim 1\%$, 5% , and 6% for Al/C, Fe/C, and Pb/C ratio, respectively, with a negligible contribution to the corresponding total systematic uncertainty.

Nuclear transparency is formally defined as the ratio of the experimentally extracted nucleon knock-out cross-section to the Plane Wave Impulse Approximation (PWIA) cross-section,

$$T_N(A) = \frac{\sigma_{exp}A(e, e'N)}{\sigma_{PWIA}A(e, e'N)}. \quad (1)$$

In the commonly used factorized approximation for large- Q^2 reactions, σ_{PWIA} is given by (see [25]):

$$\sigma_{PWIA}(e, e'N) = \frac{K}{\#N_{tar}} \cdot \sigma_{eN} \cdot \oint S_A(E, p_i) dE d^3p_i, \quad (2)$$

in which $\#N_{tar}$ is the number of relevant nucleons in the target nucleus (i.e. number of protons for $(e, e'p)$ and neutrons for $(e, e'n)$ reactions), $K = |\vec{p}_N| \cdot E_N$ is a kinematical factor, E_N is the energy of the outgoing nucleon, σ_{eN} is the off-shell electron-nucleon elementary cross section, $S_A(E, p_i)$ is the nuclear spectral function, which defines the probability for finding a nucleon in the nucleus with momentum p_i and separation energy E . $S_A(E, p_i)$ is normalized as $\int_0^\infty S_A(E, p_i) dE d^3p_i \equiv \#N_{tar}$. The limits of the integral over the spectral function in Eq. 2 should correspond to the experimental acceptance.

Under the condition that the measurements for a nucleus with A nucleons and for ^{12}C are done in equivalent kinematics, as was done in this work, their transparency ratio is given by:

$$\frac{T_N(A)}{T_N(C)} = \frac{\sigma_{exp}A(e, e'N)}{\sigma_{exp}C(e, e'N)} \cdot \frac{\oint S_C(E, p_i) dE d^3p_i}{\oint S_A(E, p_i) dE d^3p_i}, \quad (3)$$

in which the spectral functions for A and C are integrated over the same kinematical regions.

For the MF kinematics, Eq. 3 can be expressed as:

$$\frac{T_N^{MF}(A)}{T_N^{MF}(C)} = \frac{\int_0^{k_0} n_C(p_i) dp_i}{\int_0^{k_0} n_A(p_i) dp_i} \cdot \frac{\sigma_{exp}A(e, e'N)}{\sigma_{exp}C(e, e'N)}, \quad (4)$$

where $\sigma_{exp}A(e, e'N)/\sigma_{exp}C(e, e'N)$ is the measured nucleon knockout cross-section ratio discussed above and the first term is the ratio of integrals over the mean-field part of the nuclear momentum density, which, due to the large missing-energy cut, replaces the integrals over the mean-field spectral functions. The nuclear momentum density is defined as $n_A(p_i) \equiv \int_0^\infty S_A(E, p_i) dE$. The later was calculated following [18]. The integral calculations in Eq. 4 were done using three different models for

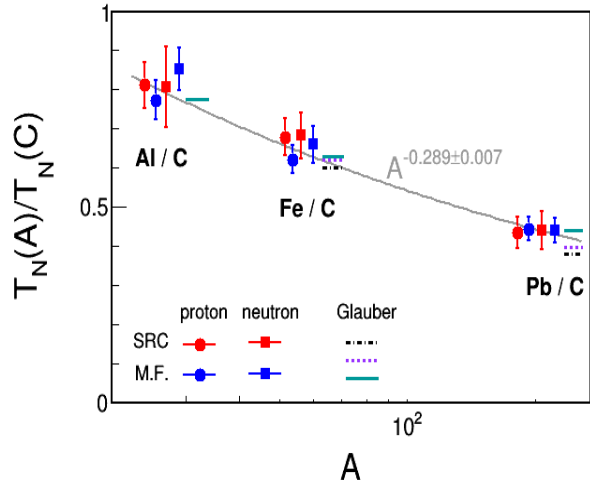


FIG. 2: The estimated transparency ratios for MF and SRC kinematics, both for protons and neutrons, together with a power law fit to a weighted average (grey line), as described in the text. For Fe and Pb nuclei, also shown are results based on three Glauber Calculations: [18] dotted line, [19] dashed line, and [20, 21] solid line.

the mean-field momentum distribution: Ciofi and Simula [26], Woods-Saxon [27], and Serot-Walecka [28] with k_0 , the upper limit of the MF momentum range, chosen to be the average between 300 MeV/ c and the Fermi sea level, $k_F = 221$; 260; 260; and 260 (280) MeV/ c for C, Al, Fe, Pb, respectively, for protons (neutrons) [29]. We assigned the half difference between the two extreme values obtained by considering the different values of k_0 and the different models as a corresponding systematic uncertainty. The values of the latter are 4.9% (3.8%), 4.2% (5.7%), and 4.3% (4.5%) for protons (neutrons) for the Al/C, Fe/C, and Pb/C ratios, respectively. The results of this calculation are consistent with those previously obtained by Hartree-Fock-Slater wave functions [18].

The transparency ratios in SRC kinematics are extracted following [10] as:

$$\frac{T_N^{SRC}(A)}{T_N^{SRC}(C)} = \frac{1}{a_2(A/C)} \cdot \frac{\sigma_{exp}A(e, e'N)/A}{\sigma_{exp}C(e, e'N)/12}, \quad (5)$$

where $a_2(A/C)$ is the relative number of $2N$ -SRC pairs per nucleon in nuclei A and C . These ratios were adapted from [30] and are based on a compilation of world data for the (e, e') cross-section ratio at large Q^2 and $x_B > 1$ with different theoretical corrections.

As shown in Fig. 1, the extracted transparency ratios are independent of nucleon momentum between 1.4 and 2.4 GeV/ c for both protons and neutrons, and for each of the three nuclei. Also shown are previous measurements for protons [13, 14, 16, 17], which are consistent with the new results. The proton knockout data also show an overall good agreement with various Glauber calcula-

tions [18–21].

The transparency ratios, averaged over nucleon momentum and type of nucleon, for each kinematics are listed in Table III. The systematic uncertainties of these estimates include the sensitivity to the event selection cuts (see Tables I and II), and a 2% uncertainty of the integrated charge. For the SRC the uncertainties also include the uncertainty of $a_2(A/C)$ (5%), and a 5% uncertainty due to the np -dominance assumption for the Pb/C case (see Ref. [10]). For the MF, the uncertainties also include the uncertainty from the MF integrals discussed above. The systematic uncertainty is independent of nucleon momentum. In Fig. 1 and elsewhere in this paper, the uncertainties shown and quoted are total uncertainties (systematic and statistical summed in quadrature), except if specifically stated otherwise.

Figure 2 shows the extracted transparency ratios, averaged over the momentum range shown in Fig. 1, as a function of the nuclear mass number. Notice that the momentum ranges are 1.64–2.34 GeV/ c (3 bins) for MF, and 1.57–2.34 GeV/ c for SRC. As mentioned above, the transparency ratios are independent of nucleon momentum in these ranges. For example, averaging the MF transparency ratios over 1.40–2.34 GeV/ c (all 4 bins) yields a value that is within 1% (much smaller than the smallest total uncertainty) of the average over 1.64–2.34 GeV/ c (last 3 bins).

Since all the four transparency ratios are consistent with each other within their experimental uncertainties, we take their weighted average for each nucleus and, following [13, 14, 16, 17], we fit them to a power law in the form of A^α . The Glauber calculation indicates the distribution of the hard process in the nucleus. Our extracted value of $\alpha = -0.289 \pm 0.007$ is consistent with the Glauber result of $\alpha = -0.288$ to -0.337 [18–21], which indicate a surface dominance of all measured reactions, also in neutron-rich nuclei like lead.

TABLE I: The $(e, e'N)$ event selection cuts for the MF kinematics. Also shown are the uncertainties of each transparency ratio due to variations in the cuts. For each nucleus, the left and the right sensitivity values are for proton and neutron knockout, respectively.

MF Cut	Cut uncertainty [%]						
	Range	Al/C	Fe/C	Pb/C			
$-0.05 < y < 0.25$	± 0.05	1.6	0.8	1.3	1.3	1.2	1.6
$0.95 < \omega < 1.7$ GeV	± 0.1 GeV	1.4	1.4	0.8	1.2	2.0	1.7
$\theta_{Nq} < 8^\circ$	$\pm 1^\circ$	1.3	1.5	1.9	1.6	1.6	1.0
$p_{miss} < 0.3$ GeV/ c	± 0.025 GeV/ c	1.2	1.2	2.0	1.3	1.8	1.5
$E_{miss} < 0.19$ GeV	± 0.02 GeV	1.9	0.8	1.8	0.9	1.9	1.4
Total:		3.4	2.6	3.6	2.9	3.9	3.1

TABLE II: Same as Table I but for the SRC kinematics. *These cuts were varied together.

SRC Cut	Cut uncertainty [%]						
	Range	Al/C	Fe/C	Pb/C			
$x_B > 1.1$	± 0.05	0.8	1.1	1.5	2.0	2.0	1.9
$0.62 < \vec{p}_N / \vec{q} < 1.1$	$*\pm 0.1$	1.4	1.4	0.8	1.2	2.0	1.7
$\theta_{Nq} < 25^\circ$	$*\pm 5^\circ$						
$m_{miss} < 1.175$ GeV/ c^2	± 0.02 GeV/ c^2	1.9	2.4	2.1	3.0	2.2	2.0
$0.4 < p_{miss} < 1$ GeV/ c	± 0.025 GeV/ c	2.2	2.3	1.9	1.6	2.6	2.3
Total:		3.6	3.8	4.1	4.7	4.6	4.4

TABLE III: The transparency ratios and their uncertainties for MF kinematics. For each nucleus, the left and the right values are for proton and neutron knockout, respectively. The first uncertainty is statistical and the second is the total.

	MF	
	$(e, e'p)$	$(e, e'n)$
Al/C	$0.771 \pm 0.017 \pm 0.051$	$0.853 \pm 0.033 \pm 0.054$
Fe/C	$0.621 \pm 0.005 \pm 0.036$	$0.660 \pm 0.015 \pm 0.047$
Pb/C	$0.442 \pm 0.010 \pm 0.029$	$0.439 \pm 0.017 \pm 0.031$

TABLE IV: Same as table III but for SRC kinematics.

	SRC	
	$(e, e'p)$	$(e, e'n)$
Al/C	$0.811 \pm 0.028 \pm 0.060$	$0.807 \pm 0.088 \pm 0.103$
Fe/C	$0.679 \pm 0.013 \pm 0.048$	$0.683 \pm 0.034 \pm 0.059$
Pb/C	$0.435 \pm 0.013 \pm 0.040$	$0.439 \pm 0.032 \pm 0.049$

In summary, we determined experimentally $A(e, e'p)$ and $A(e, e'n)$ cross-section ratios for ^{27}Al , ^{56}Fe , and ^{208}Pb nuclei relative to ^{12}C in MF and SRC kinematics. From these ratios we extracted the nuclear transparency ratios for protons and neutrons in each kinematics. Both the proton and neutron transparency ratios are independent of nucleon momentum and consistent with each other within the experimental uncertainty, for all measured nuclei. The A -dependence of the transparency ratio as well as the Glauber calculations are consistent with the hypothesis that nucleon knockout occurs on the nuclear surface.

We acknowledge the efforts of the staff of the Accelerator and Physics Divisions at Jefferson Lab that made this experiment possible. We are also grateful for many fruitful discussions with L.L. Frankfurt, M. Strikman, J. Ryckebusch, W. Cosyn, M. Sargsyan, and C. Ciofi degli Atti. The analysis presented here was carried out as part of the Jefferson-Lab Hall-B Data-Mining project supported by the U.S. Department of Energy (DOE). The research was supported also by the National Science Foundation, the Pazy Foundation, the Israel Science Foundation, the Chilean Comision Nacional de Investigacion Cientifica y Tecnologica, the French Centre National de la Recherche Scientifique and Commissariat a l'Energie Atomique, the French-American Cultural Exchange, the Italian Istituto Nazionale di Fisica Nucleare, the Na-

tional Research Foundation of Korea, and the UKs Science and Technology Facilities Council. Jefferson Science Associates operates the Thomas Jefferson National Accelerator Facility for the DOE Office of Science, Office of Nuclear Physics under contract DE-AC05-06OR23177. The raw data from this experiment are archived in Jefferson Lab's mass storage silo.

* Contact Author hen@mit.edu

† On sabbatical leave from Nuclear Research Centre Negev, Beer-Sheva, Israel

‡ Current address: Idaho State University, Pocatello, Idaho 83209

§ Current address: INFN, Sezione di Genova, 16146 Genova, Italy

- [1] D. Dutta, K. Hafidi, and M. Strikman, *Prog. Part. Nucl. Phys.* **69**, 1 (2013).
- [2] O. Hen, G. A. Miller, E. Piasetzky, and L. B. Weinstein, *Rev. Mod. Phys.* **89**, 045002 (2017).
- [3] L. B. Weinstein and S. E. Kuhn, Short distance structure of nuclei: Mining the wealth of existing Jefferson Lab data, DOE Grant DE-SC0006801 (2016).
- [4] H. Hakobyan et al., *Nucl. Instrum. Meth.* **A592**, 218 (2008).
- [5] B. A. Mecking et al., *Nucl. Instrum. Meth.* **A503**, 513 (2003).
- [6] M. Braverman, Detecting Neutrons in the CLAS Electromagnetic-Calorimeter, Tel-Aviv University M.Sc. Thesis (2014).
- [7] M. Duer et al. (CLAS Collaboration), *Nature* **560**, 617 (2018).
- [8] A. Aste, C. von Arx, and D. Trautmann, *Eur. Phys. J.* **A26**, 167 (2005).
- [9] N. Fomin et al., *Phys. Rev. Lett.* **108**, 092502 (2012).
- [10] O. Hen et al. (CLAS Collaboration), *Phys. Lett.* **B722**, 63 (2013).
- [11] O. Hen et al. (CLAS Collaboration), *Science* **346**, 614 (2014).
- [12] D. F. Geesaman et al., *Phys. Rev. Lett.* **63**, 734 (1989).
- [13] T. G. O'Neill et al., *Phys. Lett.* **B351**, 87 (1995).
- [14] G. Garino et al., *Phys. Rev. Lett.* **80**, 5072 (1998).
- [15] T. W. Donnelly, *NATO Sci. Ser. II* **53**, 19 (2002).
- [16] D. Abbott et al., *Phys. Rev. Lett.* **80**, 5072 (1998).
- [17] K. Garrow et al., *Phys. Rev.* **C66**, 044613 (2002).
- [18] L. Frankfurt, M. Strikman, and M. Zhalov, *Phys. Lett.* **B503**, 73 (2001).
- [19] V. R. Pandharipande and S. C. Pieper, *Phys. Rev.* **C45**, 791 (1992).
- [20] C. Colle and W. Cosyn, *Phys. Rev. C* **93**, 034608 (2016).
- [21] W. Cosyn, Private communication.
- [22] M. Sargsyan, Report No YERPHI-1331-15-91 (1991).
- [23] K. Egiyan et al. (CLAS Collaboration), *Phys. Rev. C* **68**, 014313 (2003).
- [24] K. Egiyan et al. (CLAS Collaboration), *Phys. Rev. Lett.* **96**, 082501 (2006).
- [25] T. De Forest, *Nucl. Phys.* **A392**, 232 (1983).
- [26] C. Ciofi degli Atti and S. Simula, *Phys. Rev. C* **53**, 1689 (1996).
- [27] M. Vanhalst, J. Ryckebusch, and W. Cosyn, *Phys. Rev. C* **86**, 044619 (2012).
- [28] R. J. Furnstahl, B. D. Serot, and H.-B. Tang, *Nucl. Phys.* **A615**, 441 (1997), [Erratum: *Nucl. Phys.*A640,505(1998)].
- [29] E. Moniz et al., *Phys. Rev. Lett.* **26**, 445 (1971).
- [30] B. Schmoolker et al. (CLAS Collaboration), submitted (2018).